Dalton Transactions

Accepted Manuscript

ROYAL SOCIETY OF CHEMISTRY

www.rsc.org/dalton

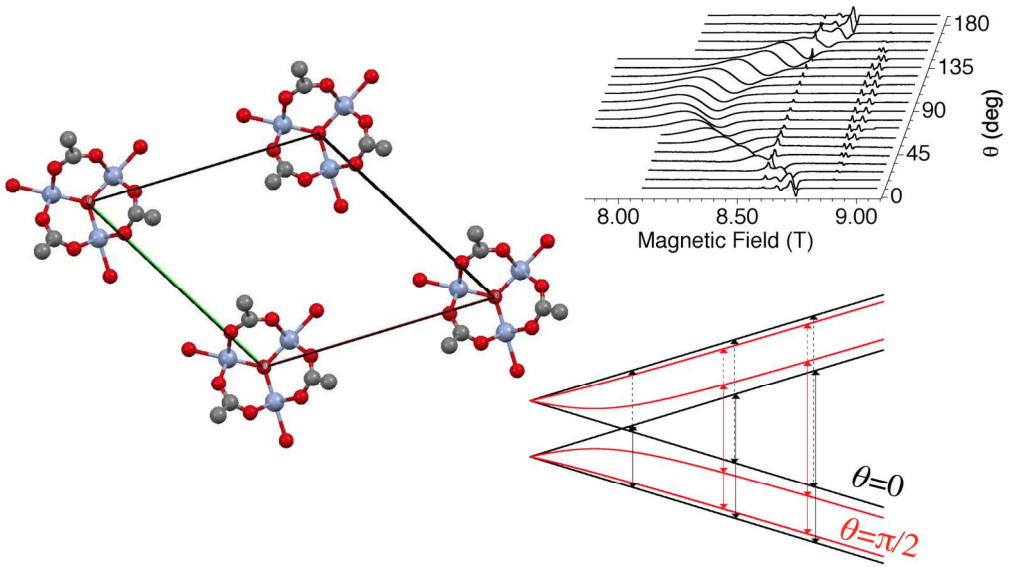

Dalton Transactions

RSCPublishing

ARTICLE

Effects of the Dzyaloshinskii-Moriya interaction in $[Cr_3O(O_2C^tBu)_6(H_2O)_3](O_2C^tBu)\ HO_2C^tBu\cdot 2EtOH$ triangular spin clusters detected by specific heat and multi-frequency electron spin resonance

sCite this: DOI: 10.1039/xoxxoooooox

Received ooth January 2012,
Accepted ooth January 2012

DOI: 10.1039/xoxxoooooox

www.rsc.org/

Alberto Ghirri[a,*], Johan van Tol[b], Inigo Vitorica-Yrezabal,[c] Grigore A. Timco[c] and Richard E. P. Winpenny[c].

An oxo-centered $[Cr_3O(O_2C^tBu)_6(H_2O)_3](O_2C^tBu)\ HO_2C^tBu\cdot 2EtOH$ triangular cluster has been synthesized and its magnetic properties have been studied by means of complementary techniques, namely magnetometry, specific heat and multi-frequency Electron Paramagnetic Resonance (EPR). Measurements on oriented single-crystals evidenced the presence of anisotropy that we attributed to the combined effect of Dzyaloshinskii-Moriya exchange interaction and distortion. By means of a minimal set of parameters, we show that a simple analytical model well describes the main features of the full set of experimental data.

Introduction

A spin triangle with antiferromagnetic nearest-neighbour exchange represents the simplest paradigm of spin frustrated system: three half-integer spins cannot all be anti-parallel aligned and this may result in a degenerate ground state [1]. The extensive investigation of triangular spin clusters [2], however, has evidenced that the magnetic properties of these systems are very sensitive to small interactions, such as Dzyaloshinskii-Moriya exchange or Jahn-Teller distortion, that are beyond the Heisenberg model and that have the effect of lifting the ground state degeneracy [3, 4]. Owing to their particular properties, spin triangles have been proposed for the encoding of spin qubits [5] or for the observation of the spin-electric effect [6].

The Dzyaloshinskii-Moriya interaction [7], also known as antisymmetric exchange, manifests the tendency of the spins to be oriented perpendicular to each other, instead of (anti)parallel as for the isotropic Heisenberg exchange [8]. This interaction is at the basis of spin canting in weak ferromagnetism and is relevant for multiferroicity [9-11]. Its effects have been also invoked to explain particular features of molecular nanomagnets, such as forbidden tunnelling steps in single-molecule magnets [12], higher order anisotropy in Ni_4 [13], EPR transitions in Cu_3 [14, 15] and V_{15} [16]. Recently, the antisymmetric exchange has been exploited to introduce anisotropy in a Ru_2Mn heterometallic triangle [17].

The synthesis of the first Cr_3 cluster dates back to 1908 [18], and many variants of the Cr_3 triangle have been reported ever since [2, 19-21]. Crystallographic data, normally taken at room temperature, often indicate that the Cr^{3+} ions are positioned at the vertices of an almost equilateral triangle. Measurements at low temperature suggest that distortions of the molecular structure occur [19, 22, 23], which lower the trigonal symmetry. In such a way the Heisenberg model accounts for the splitting in two doublets of the otherwise 4-fold degenerate ground state. Indeed, the zero-field splitting has been ubiquitously detected by means of experiments in zero magnetic field [24, 25]. To obtain a quantitative agreement with the experimental data, different theoretical models have been proposed [20-22, 24-27]. The Dzyaloshinskii-Moriya interaction, which has been successfully introduced in Cu_3 to describe the low-temperature susceptibility and the observed EPR transitions [14], provides the most plausible explanation for the anisotropic *g*-factors observed in different Cr_3 triangles [2, 20, 21].

Here we report the synthesis of single-crystals of $[Cr_3O(O_2C^tBu)_6(H_2O)_3](O_2C^tBu)\ HO_2C^tBu\cdot 2EtOH$, hereafter for commodity referred as Cr_3, and the study of the magnetic properties by means of complementary techniques such as magnetometry, specific heat and multi-frequency electron paramagnetic resonance (EPR). Our results evidence the effects of the Dzyaloshinskii-Moriya interaction and find excellent agreement with existent analytical models that include both Dzyaloshinskii-Moriya exchange and distortion [27-29].

Synthesis and structural description

The compound $[Cr_3O(O_2C^tBu)_6(H_2O)_3](O_2C^tBu)$ was synthesised by reaction of hydrated chromium nitrate with pivalic acid at 160° C for around 5 hours, until all NO_2 gas evolution had ceased. The compound was recrystallized from EtOH, giving crystals of the solvate $[Cr_3O(O_2C^tBu)_6(H_2O)_3](O_2C^tBu)$. HO_2C^tBu. 2 EtOH. The crystals form in a hexagonal space group, which allows the cationic cluster $[Cr_3O(O_2C^tBu)_6(H_2O)_3]^+$ to sit on a crystallographic three-fold axis (Figure 1). The Cr…Cr distances within the equilateral triangle are 3.2815(5) Å. The triply bridging oxide sits on the three-fold axis. The local symmetry of each chromium is a distorted octahedron with six bonds to O atoms. One from μ_3- bridged oxygen atom at the center of the triangle, four from six pivalate ligands bridge the edges of the triangle, and one from three water molecules in terminal sites of the metal ions. The charge of $[Cr_3O(O_2C^tBu)_6(H_2O)_3]^+$ is balanced by an additional pivalate that forms intermolecular hydrogen bonds to trinuclear units in the lattice. X-ray data for compound $[Cr_3O(O_2C^tBu)_6(H_2O)_3](O_2C^tBu)$ HO_2C^tBu .2EtOH was collected at a temperature of 150 K

Magnetic measurements

The susceptibility-*vs*-temperature curve was measured on a polycrystalline sample of Cr_3 in the temperature range 2 K < T < 300 K (Figure 2a). The χT product shows a progressive decrease with decreasing temperature, as expected for antiferromagnetic exchange interactions (Figure 2b). The plateau at 0.35 emu K mol^{-1}, reached for T~4 K, is compatible with a spin 1/2 ground state. Below 4 K, a downturn of the χT product is observed, which become more pronounced in the χT-vs-T curves measured in applied magnetic field up to 7 T (Figure 2b). Figure 2c shows the magnetization curve at 2 K measured as a function of the external field (B).

Specific heat

Specific heat (C) was measured as a function of temperature on single crystals of Cr_3 (Figure 3). In zero field, the lattice contribution (C_{latt}) dominates the specific heat curve at high temperature. In contrast to the chloride salt Cr_3 triangle [22], for $[Cr_3O(O_2C^tBu)_6(H_2O)_3][O_2C^tBu]$ we did not observe any evidence of phase transition in the range 0.3-300 K. For T<6 K a Schottky anomaly peaked at T≃2 K becomes clearly visible above C_{latt}. To evaluate the separated contribution, we estimated the lattice specific heat as [30]:

$$\frac{C_{latt}}{R} = 234\left(\frac{T}{\theta_D}\right)^{\alpha}, \quad (1)$$

where R=8.314 J K^{-1} mol^{-1}, θ_D=40 K and α=2.7 (dashed line in Figure 3). For two degenerate energy levels, the Schottky anomaly can be expressed as:

$$\frac{C_0}{R} = \rho\left(\frac{T_0}{T}\right)^2 \frac{\exp\left(\frac{T_0}{T}\right)}{\left[1+\rho\exp\left(\frac{T_0}{T}\right)\right]^2}, \quad (2)$$

where ρ is the degeneracy ratio of the energy levels. The best fit of C/R-vs-T is obtained for ρ=1 and T_0=5.2 K (dash-dot line in Figure 3). This indicates the presence of two doublets separated by 5.2 K. Note that below 1 K the specific curve tends to zero, as expected for a Kramers doublet.

Figure 4 shows the C/R-vs-T curves measured under applied B. Two different orientations were measured, which correspond to **B** parallel to the c-axis (θ = 0), and **B** lying parallel in the triangle plane (θ = π/2). For B = 0.5 T an additional Schottky anomaly appears at low temperature that, for increasing field, is shifted toward higher T according to the Zeeman energy of a spin 1/2 state. Note that for each field the $C(B)$ curves measured for θ = 0 and π/2 show a different behaviour, clearly stating the presence of anisotropic effects.

High frequency EPR

Continuous wave EPR measurements were carried out at ~120, 241 and 336 GHz on an oriented single-crystal of Cr_3. Figure 5a shows a field sweep in the range 0-12 T. The temperature dependence of the EPR resonances found between 8.2 and 9.2 T is shown in Figure 5b. At 15 K at least three peaks are visible. They reduce, for T=10 K, to two well-defined resonances at 8.677 and 8.738 T, which correspond respectively to effective g-factors of 1.985 and 1.971. For decreasing temperature the former progressively weakens, suggesting that its origin is in the higher lying doublet. We can thus assign g_1=1.971 to the lower doublet and g_2=1.985 to the higher doublet.

A series of 241 GHz EPR spectra were measured for different θ angles (Figure 6a) at 4 K. The rotation about an axis in the ab plane give rise to the progressive overlap of the two resonances measured for θ = 0 and to the formation of a broad derivative peak for θ = π/2. This is also accompanied by the decrease of the intensity of the EPR signal and suggests the presence of two inequivalent orientations of the Cr_3 clusters in the ab plane. The resonance position shifts to ~8.2 T at θ = π/2, which corresponds to an increase of the effective g-factor to 2.10. Weaker resonances are visible also at about 8.9 T whose origin has not been clearly identified.

To probe other regions of the energy level diagram we acquired EPR spectra also at 336 GHz and 120 GHz. For θ = 0, the shift of the field position of the EPR resonances is linear according to $h\nu/g_{1(2)}\mu_B$ and confirms the values of g_1 and g_2 extracted at 241 GHz. Conversely, for $\theta \neq 0$ the shift is not linear. At 336 GHz, the resonance peaks shift from 12.1 T (θ = 0) to 11.8 T (θ = π/2) (Figure 6b), thus the latter corresponds to an effective g-factor of 2.03. At 120 GHz the EPR signal rapidly disappears as the magnetic field is turned off-axis by a small angle (Figure 6c). This is evidence that for B~4 T the resonance condition is no longer satisfied when the triangle axis is progressively rotated perpendicular to the field.

Discussion

Although crystallographic data taken at intermediate temperature point to an almost perfect trigonal symmetry of the Cr_3 cluster, for this family of compounds the presence of distortions of the molecular structure is well documented by low temperature measurements [2, 19-23, 31]. For an isosceles triangle, two exchange constants are introduced and the isotropic Heisenberg-Dirac-vanVleck Hamiltonian reads:

$$H_{HDVV} = -J\,(\boldsymbol{S_{A1}}\cdot\boldsymbol{S_B} + \boldsymbol{S_{A2}}\cdot\boldsymbol{S_B}) - J'(\boldsymbol{S_{A1}}\cdot\boldsymbol{S_{A2}}) \quad (3)$$

where S_{A1}= S_{A2}= S_B=3/2 is the spin of the Cr^{3+} ions and J, J' are antiferromagnetic. By defining $\boldsymbol{S'} = \boldsymbol{S_{A1}} + \boldsymbol{S_{A2}}$ and $\boldsymbol{S} = \boldsymbol{S'} + \boldsymbol{S_B}$, from Eq. 1 the ground state doublets $|S,S'\rangle$=$|1/2,1\rangle$ and $|1/2,2\rangle$, are split at zero field of $2\delta=2|J-J'|$. The Van Vleck susceptibility can be calculated by introducing the Zeeman term as first-order perturbation:

$$H_Z = \mu_B[g_A(\boldsymbol{S}_{A1} + \boldsymbol{S}_{A2}) + g_B\boldsymbol{S}_B]\cdot\boldsymbol{B} \quad (4)$$

where g_A and g_B are respectively the local g-factors of S_{A1}(S_{A2}) and S_B [31]. The susceptibility thus results:

$$\chi = \frac{N_A{\mu_B}^2}{3k_BT}\frac{\sum_{S'=0}^{2S_A}\sum_{S=|S'-S_B|}^{S'+S_B} g_{S,S'}{}^2 S(S+1)(2S+1)\exp[-E(S,S')/k_BT]}{\sum_{S'=0}^{2S_A}\sum_{S=|S'-S_B|}^{S'+S_B}(2S+1)\exp[-E(S,S')/k_BT]} \quad (5)$$

where $g_{S,S'}$ are the effective g-factors associated to the $E(S, S')$ state. By means of Eq. 5 we fitted the experimental susceptibility curve and we obtained J/k_B = −31±1 K and J'/k_B = −33±1 K, with a reduced effective g-factor $g_{S,S'} = g_{eff}$ = 1.94 (dashed lines in Figure 2a and 2b). These parameters are close to those reported for similar variants of Cr_3 triangles [2, 21]. The calculated energy splitting $2\delta/k_B$ =$2|J-J'|/k_B$ =4±3 K, is not incompatible with T_0 = 5.2 K. This approach, however, fails to reproduce the anisotropic behaviour shown by single-crystal specific heat and EPR measurements (Figure 4 and 6).

To introduce anisotropy in the spin Hamiltonian firstly we have to consider the effects of the Cr^{3+} single ion anisotropy. A Cr^{3+} ion in distorted octahedral symmetry usually shows isotropic g_{Cr} [32] and nearly axial d_{Cr} [33]. Intrinsically these parameters cannot provide either an adequate fit of the specific heat curves or account for the angular dependence of multi-frequency EPR spectra. The anisotropic g-factor, observed by X-band EPR on closely related Cr_3 triangular clusters, has been attributed to the effect of the Dzyaloshinskii-Moriya interaction [27, 20, 21]. For a slightly distorted trigonal system, the antisymmetric exchange

$$H_{DM} = \sum_{ij}\boldsymbol{G_{ij}}\boldsymbol{S_i}\times\boldsymbol{S_j} \quad (6)$$

can be assumed to be parallel to the trigonal axis z [7, 28] and the antisymmetric tensor be reduced to a scalar parameter $G=G_{zz}$. By defining $\Delta = \sqrt{\delta^2 + G^2}$, from $\boldsymbol{H} = H_{HDVV} + H_{DM} + H_Z$ the energies of the ground state doublets that result are:

$$E_1^{\pm} = -\tfrac{1}{2}g'\mu_B B \pm \left[G^2 + \left(\delta - \tfrac{1}{2}g"\mu_B B\right)^2\right]^{1/2} \quad (7a)$$

$$E_2^{\pm} = \tfrac{1}{2}g'\mu_B B \pm \left[G^2 + \left(\delta + \tfrac{1}{2}g"\mu_B B\right)^2\right]^{1/2} \quad (7b)$$

for θ=0 and

$$E_1^{\pm} = -\tfrac{1}{2}g"\mu_B B \pm \left[G^2 + \left(\delta - \tfrac{1}{2}g'\mu_B B\right)^2\right]^{1/2} \quad (8a)$$

$$E_2^{\pm} = \tfrac{1}{2}g"\mu_B B \pm \left[G^2 + \left(\delta + \tfrac{1}{2}g'\mu_B B\right)^2\right]^{1/2} \quad (8b)$$

for θ=π/2, where $g' = (2g_A + g_B)/3$ and $g" = 4(g_A - g_B)/3$ [28]. The specific heat $C(B)$-vs-T curves can be calculated as:

$$\frac{C}{R} = \frac{\sum_i E_i{}^2\exp(E_i/k_BT)\sum_i\exp(E_i/k_BT) - [\sum_i E_i\exp(E_i/k_BT)]^2}{(k_BT)^2[\sum_i\exp(E_i/k_BT)]^2} \quad (9)$$

where $E_i = E_1^{\pm}, E_2^{\pm}$. Good agreement with the experimental data was obtained with δ/k_B=1.8±0.1 K, G/k_B=1.8±0.1 K and $g_A = g_B = 1.97$, which reproduce the whole set of $C(B,\theta)$-vs-T curves (Figures 3 and 4). Within this model [14], the susceptibility

$$\chi = \frac{kT}{BZ}\frac{\partial Z}{\partial B} \quad (10)$$

where Z is the partition function, can be calculated for different θ angles and averaged to reproduce the experimental curve taken on a polycrystalline sample. By means of the parameters obtained from the specific heat, Eq. 10 accounts for the downturn of χT at low temperature and for its evolution in applied B (Figure 2b). This is confirmed in Figure 2c by the correspondence between the calculated magnetization at 2 K and the experimental data.

We thus calculated the pattern of the energy levels as a function of B (Figure 7). The ground state doublets are split of $2\Delta/k_B=T_0$=5.2 K at zero magnetic field and for θ=0 the field dependence is linear. For θ=π/2 the antisymmetric term gives rise to non-linear dependence of the Zeeman levels and turns on the inter-doublet mixing between E_1^- and E_2^+ [26]. Below 1 T the field dependence of the energy levels at θ=π/2 can be approximated as linear with a reduced effective g-factor ≃1.3. This behaviour is consistent to the outcome of X-band EPR studies reported in the literature for different types of Cr_3 triangles [2, 20, 21, 26, 34].

Direct verification of the calculated Zeeman diagram can be carried out by multi-frequency EPR spectroscopy. High-frequency spectra at 241 and 336 GHz provide photons with $h\nu > \Delta$, while at 140 GHz their energy is in the range $h\nu \sim \Delta$. X-band spectra ($h\nu < \Delta$) have been reported in Ref. [34]. In Table 1 are listed the EPR resonances observed at low

temperature for θ = 0 and $\pi/2$. The experimental $B_{exp}(\theta)$ are compared with those calculated from Eq. 7 and 8 [$B_{th}(\theta)$]. The two EPR resonances obtained with g_1=1.971 and g_2=1.985 for ν=120, 241 and 336 GHz and θ=0 (Figure 5 and 6) can be reproduced by assuming only slightly different $g_{A1,\ A2}$=1.980 and g_B=1.976. The experimental $B_{exp}(\theta)$ are consistent with the calculated $B_{th}(\theta)$ within ±1% of discrepancy. The observed EPR resonances are plotted in Figure 7 in correspondence to the observed resonance field [$B_{exp}(\theta)$]. The comparison with the calculated Zeeman diagram well explains the non-trivial dependence of $B_{exp}(\theta)$ at various frequencies. In particular, the mixing of the energy levels for $\theta \neq 0$ accounts for the vanishing of the EPR signal for ν=120 GHz and off axis orientation. All the observed EPR resonances correspond to intra-doublet transitions and we report no evidence of inter-doublet transitions for this particular Cr_3 derivative (Figure 5a). This quenching of the inter-doublet resonances is consistent with the transition probability calculated in Ref. [29] for a triangle with isosceles distortion.

EPR resonance	ν (GHz)	Θ (rad)	$B_{exp}(\theta)$ (T)	$B_{th}(\theta)$ (T)
E^-_2- E^-_1 E^+_2- E^+_1	9.215	0	0.335±0.005	0.333
E^-_2- E^-_1 E^+_2- E^+_1	9.215	$\pi/2$	0.45±0.05	0.480
E^+_2- E^+_1	120.496	0	4.347±0.003	4.339
E^-_2- E^-_1	120.496	0	4.366±0.003	4.353
E^-_2- E^-_1 E^+_2- E^+_1	240.992	$\pi/2$	8.215±0.003	8.209
E^+_2- E^+_1	240.992	0	8.670±0.003	8.677
E^-_2- E^-_1	240.992	0	8.731±0.003	8.710
E^-_2- E^-_1 E^+_2- E^+_1	336.000	$\pi/2$	11.793±0.003	11.778
E^+_2- E^+_1	336.000	0	12.050±0.003	12.098
E^-_2- E^-_1	336.000	0	12.128±0.003	12.144

Table 1. List of the EPR resonances observed at low temperature. The error bar associated with $B_{exp}(\theta)$ reflects the ΔB measured between upward and downward field sweeps. A larger error bar is associated for ν=9.215 GHz and $\theta = \pi/2$ due to the broad absorption spectrum reported in Ref. [34].

Conclusions

In conclusion, we investigated oxo-centered Cr^{3+} triangles by means of complementary experimental techniques. Single-crystal specific heat and EPR measurements display the effects of anisotropy and are consistent with an analytical model that includes both antisymmetric exchange and distortion. The inclusion of the Dzyaloshinskii-Moriya term explains the non-trivial angle dependence of multi-frequency EPR spctra. The zero-field splitting of the ground state doublets (Δ/k_B = 5.2 K) arises from the equal contribution of distortion (δ/k_B = 1.8 K) and antisymmetric exchange (G/k_B = 1.85 K). These results show the effects of the interplay between these competing interactions and can be useful for understanding other classes of magnetic systems.

Experimental

Synthetic procedures

All manipulations were performed under aerobic conditions. All chemicals and solvents were purchased from commercial sources and used without further purification.

$[Cr_3O(O_2C^tBu)_6(H_2O)_3](O_2C^tBu)\ HO_2C^tBu$ (1)

Chromium nitrate nonahydrate ($Cr(NO_3)_3 \cdot 9H_2O$, 10.0 g, 25 mmol) and pivalic acid (50.0 g, 490 mmol) were heated with stirring from room temperature (R.T.) to 160° C in a two neck flask fitted with a distillation condenser to the middle neck and the second connected to a slow flow of air to carry away the NO_2 generated in the reaction, which is removed through the condenser directly into an aqueous solution of $NaHCO_3$. After the elimination of NO_2 was complete (~4-5 h until no more reddish-brown gas is observed) the flask was cooled to 80- 85°C and ethanol (100 ml) was added and then the solution was further diluted over a period of 15 min with 40 ml of water and left to cool to room temperature and stirred at room temperature overnight. A green microcrystalline product was obtained, which was collected by filtration, washed with toluene then with diethyl ether and dried in air.

Yield: 8.07 g (93%.). Found, %: Cr, 14.65, C, 45.06; H, 8.15.. Calc. for, $C_{40}H_{79}Cr_3O_{20}$ %: Cr, 15.06, C, 46.37; H, 7.69.

ESI-MS (sample dissolved in MeOH, run in MeOH) *m/z*: + 874 $[Cr_3O(O_2C^tBu)_6(MeOH)_3]^+$ (100 %), +842 $[Cr_3O(O_2C^tBu)_6(MeOH)_2]^+$, + 810 $[Cr_3O(O_2C^tBu)_6(MeOH)]^+$

$[Cr_3O(O_2C^tBu)_6(H_2O)_3](O_2C^tBu)\ HO_2C^tBu \cdot 2EtOH$

1 (0.7g), pivalic acid (1.4g) ethanol (40 ml), and H_2O (10 ml), stirred at 60°C for 15-20 min. Obtained solution was allowed to slowly evaporate at ambient temperate over a period of several days. Dark green crystals were separated from the solution by decantation and washed with cold EtOH. Yield ~90 %

The crystals were identified by X-ray crystallography as $[Cr_3O(O_2C^tBu)_6(H_2O)_3](O_2C^tBu)\ HO_2C^tBu \cdot 2EtOH$.

Found, %: Cr, 13.91, C, 47.22; H, 8.36; ;. Calc. for, $C_{44}H_{91}Cr_3O_{22}$ %: Cr, 13.83, C, 46.84; H, 8.13

ESI-MS (sample dissolved in MeOH, run in MeOH the same as for 1.

Magnetic studies

Susceptibility and measurements were carried out on powder samples using a Quantum Design PPMS measurement system. No frequency dependence was observed in ac susceptibility measurements with an excitation field of 1 mT. Measurements in finite applied magnetic field were taken with the dc extraction technique. Specific heat experiments were carried out on a ^{3}He refrigerator with the two-tau relaxation technique. The experimental data was taken on 5 single crystals of Cr_3 (mass 1 mg) glued on the

calorimeter by means of Apiezon N grease. Specific heat-vs-temperature curves were measured under applied magnetic field with the crystals aligned respect to the field direction (θ = 0, π/2).

Continuous wave EPR experiments were carried out at the National High Magnetic Field Laboratory (NHMFL), in Tallahassee Florida, USA. The spectrometer used employs a superheterodyne quasi-optical bridge with a 40 mW solid-state source [35]. In situ rotations of the hexagonal crystal were carried out by means of a rotating sample holder mounted with its axis perpendicular to a 12.5 T superconducting solenoid. The sweep rate was 4 mT/s. Multi-frequency spectra were taken at 120.496, 240.992 and 336.000 GHz.

Analytical data were obtained by the Microanalysis laboratory at the University of Manchester.

Electrospray Ionization Mass Spectrometry (ESI-MS) were carried out by the Mass Spectrometry Service at the University of Manchester. ESI-MS spectra were recorded on Micromass "QTOF Micro" quadrupole time of flight mass spectrometer.

Crystallography

Data Collection. X-ray data for compound $[Cr_3O(O_2C^tBu)_6(H_2O)_3](O_2C^tBu)$ HO_2C^tBu ·2EtOH was collected at a temperature of 150 K using a using Mo-K_α radiation (λ = 0.71073 Å) on an Agilent Supernova, equipped with an Oxford Cryosystems Cobra nitrogen flow gas system. Data were measured using CrysAlisPro suite of programs.

Crystal structure determinations and refinements. X-ray data were processed and reduced using CrysAlisPro suite of programs. Absorption correction was performed using empirical methods based upon symmetry-equivalent reflections combined with measurements at different azimuthal angles [36]. The crystal structure was solved and refined against all F^2 values using the SHELXTL suite of programs [37]. Atoms were refined anisotropically. H-atoms were placed in calculated positions refined using idealized geometries (riding model) and assigned fixed isotropic displacement parameters. The C-C distances of the pivalate ligands were restrained to be the same using SADI and DFIX commands. The atomic displacement parameters (adp) of the ligands have been restrained using RIGU and SIMU commands.

Table S1. Crystallographic information for $[Cr_3O(O_2C^tBu)_6(H_2O)_3](O_2C^tBu)$ HO_2C^tBu ·2EtOH

Crystal colour	green
Crystal size (mm)	0.35 × 0.35 × 0.35
Crystal system	Hexagonal
Space group, Z	$P6_3/mmc$, 2
$a = b$ (Å)	12.2920(6)
c (Å)	22.719(1)
V (Å^3)	2972.8(3)
Density (Mg.m^{-3})	1.260
Temperature (K)	150
μ(Mo-Kα) (mm^{-1})	0.607
2Θ range (°)	6.602 to 58.336
Reflns collected	7877
Independent reflns used in refinement, n	1428
L.S. parameters, p	150
No. of restraints, r	121
$R1$ $(F)^a$ $I > 2.0\sigma(I)$	0.0732
$wR2(F^2)$,[a] all data	0.2107
$S(F^2)$,[a] all data	1.093

[a] $R1(F) = \Sigma(|F_o| - |F_c|)/\Sigma|F_o|$; [b] $wR^2(F^2) = [\Sigma w(F_o^2 - F_c^2)^2/\Sigma wF_o^4]^{½}$; [c] $S(F^2) = [\Sigma w(F_o^2 - F_c^2)^2/(n + r - p)]^{½}$

The crystallographic data and experimental details of the structural refinement for the X-ray crystal structure reported in this paper has been deposited at the Cambridge Crystallographic Data Centre, under deposition number CCDC 1059922. These data can be obtained free of charge at (http://www.ccdc.cam.ac.uk/data_request/cif).

Acknowledgements

The authors acknowledge M. Affronte, S. Hill and F. Troiani for very useful discussions. This work was funded by FIRB project RBFR12RPD1 of the Italian Ministry of Research, EPSRC (UK) and by the US AFOSR/AOARD program, contract FA2386-13-1-4029. The National High Magnetic Field Laboratory is supported by NSF Cooperative Agreement No. DMR-1157490 and by the State of Florida.

Notes and references

[a] Istituto Nanoscienze-CNR, via G. Campi 213A, 41125 Modena, Italy.
[b] National High Magnetic Field Laboratory, Tallahassee, Florida 32310, United States.
[c] School of Chemistry and Photon Science Institute, University of Manchester, Oxford Road, Manchester M13 9PL, United Kingdom.
E-mail:alberto.ghirri@nano.cnr.it

1. O. Kahn, *Chem. Phys. Lett.* 1997, **265**, 109-114.
2. R. Cannon and R. White, *Prog. Inorg. Chem.* 1988, **36**, 195–298.
3. P. Kogerler, B. Tsukerblat and A. Muller, *Dalton Trans.* 2010, **39**, 21-36.
4. J. Schnack, *Dalton Trans.*, 2010, **39**, 4677–4686.
5. S. Carretta, P. Santini, G. Amoretti, F. Troiani and M. Affronte, *Phys. Rev. B*, 2007, **76**, 024408.
6. M. Trif, F. Troiani, D. Stepanenko and D. Loss, *Phys. Rev. Lett.*, 2008, **101**, 217201.
7. I. E. Dzyaloshinskii, *Sov. Phys. JETP*, 1957, **5**, 1259-1262; T. Moriya, *Phys. Rev.*, 1960, **117**, 635; T. Moriya, *Phys. Rev.*, 1960, **120**, 91-98.
8. A. P. Ginsberg, *Inorg. Chim. Acta Rev.*, 1971, **5**, 45-68.
9. R. Ramesh and N. A. Spaldin, *Nat. Mater.*, 2007, **6**, 21-29.
10. P. Lunkenheimer, J. Müller, S. Krohns, F. Schrettle, A. Loidl, B. Hartmann, R. Rommel, M. de Souza, C. Hotta, J. A. Schlueter and M. Lang, *Nat. Mater.*, 2012, **11**, 755-758.

11. V. E. Dmitrienko, E. N. Ovchinnikova, S. P. Collins, G. Nisbet, G. Beutier, Y. O. Kvashnin, V. V. Mazurenko, A. I. Lichtenstein and M. I. Katsnelson, *Nat. Phys.*, 2014, **10**, 202-206.
12. M. I. Katsnelson, V. V. Dobrovitski, B. N. Harmon, *Phys. Rev. B* 1999, **59**, 6919; I. Chiorescu, R. Giraud, A. G. M. Jansen, A. Caneschi, B. Barbarba, *Phys. Rev. Lett*. 2000, **85**, 4807; C. M. Ramsey, E. del Barco, S. Hill, S. J. Shah, C. C. Beedle, D. N. Hendrickson, *Nat. Phys.*, 2008, **4**, 277; S. Bahr, C. J. Milios, L. F. Jones, E. K. Brechin, V. Mosser, W. Wernsdorfer, *Phys. Rev. B*, 2008, **78**, 132401.
13. N. Kirchner, J. van Slageren, B. Tsukerblat, O. Waldmann, and M. Dressel, *Phys. Rev. B*, 2008, **78**, 094426.
14. B. S. Tsukerblat, B. Ya. Kuyavskaya, M. I. Belinskii, A. V. Ablov, V. M. Novotortsev and V. T. Kalinnikov, *Theor. Chim. Acta*, 1975, **38**, 131-138.
15. K.-Y. Choi, Z. Wang, H. Nojiri, J. van Tol, P. Kumar, P. Lemmens, B. S. Bassil, U. Kortz, and N. S. Dalal, *Phys. Rev. Lett.* 2012, **108**, 067206; S. Ferrer, F. Lloret, E. Pardo, J. M. Clemente-Juan, M. Liu-Gonzaĺez and S. García-Granda, *Inorg. Chem.* 2012, **51**, 985-1001.
16. B. Tsukerblat, A. Tarantul and A. Muller, *J. Chem. Phys.*, 2006, **125**, 054714; M. Martens, J. van Tol, N. S. Dalal, S. Bertaina, B. Barbara, B. Tsukerblat, A. Muller, S. Garai, S. Miyashita, and I. Chiorescu, *Phys. Rev. B*, 2014, **89**, 195439.
17. S. A. Magee, S. Sproules, A.-L. Barra, G. A. Timco, N. F. Chilton, D. Collison, R. E. P. Winpenny, and E. J. L. McInnes, *Angew. Chem. Int. Ed.*, 2014, **53**, 5310 –5313.
18. R. F. Weinland, 1908, **41**, 3236–3245; A. Werner, 1908, **41**, 3447–3465; B. N. Figgis, B, G. B. Robertson, *Nature* 1965, **205**, 694–695.
19. R. D. Cannon, U. A. Jayasooriya, F. E. Sowrey, C. Tilford, A. Little, J. P. Bourke, R. D. Rogers, J. B. Vincent and G. J. Kearley, *Inorg. Chem.* 1998**, 37***,* 5675-5677.
20. A. Vlachos, V. Psycharis, C. P. Raptopoulou, N. Lalioti, Y. Sanakis, G. Diamantopoulos, M. Fardis, M. Karayanni, G. Papavassiliou and A. Terzis, *Inorg. Chim. Acta*, 2004, **357**, 3162–3172.
21. A. Figuerola, V. Tangoulis, J. Ribas, H. Hartl, I. Bru1dgam, M. Maestro and C. Diaz, *Inorg. Chem.* 2007, **46**, 11017−11024.
22. M. Sorai, M. Tachiki, H. Suga and S. Seki, *J. Phys. Soc. Japan*, 1971, **30**, 750-759.
23. K. J. Schenk and H. U. Güdel, *Inorg. Chem.*, 1982, **21**, 2253-2256.
24. M. Nakano, T. Wakamatsu, M. Sorai and H. Suga, *J. Phys. Chem. Solids*, 1988, **49**, 987-992.
25. U. A. Jayasooriya R. D. Cannon. R. P. White, J. A. Stride, R. Grinter, and G. J. Kearley, *J. Chem. Phys.*, 1993, **98**, 9303-9310.
26. Y. V. Rakitin, Y. V. Yablokov, and V. V. Zelentsov, *J. Magn. Reson.*, 1981, **43**, 288-301.
27. B. S. Tsukerblat, M. I. Belinskii, B. Ya. Kuyavskaya and V. E. Fainzilberg, *Chem. Phys. Lett.*, 1983, **98**, 149-151.
28. B. S. Tsukerblat, B. Ya. Kuyavskaya, V. E. Fainzilberg and M. I. Belinskii, *Chem. Phys.*, 1984, **90**, 361-371.
29. A. I. Shames and M. I. Belinsky, *Phys. Stat. Sol. (b)*, 1997, **203**, 235-245.
30. M. Evangelisti, F. Luis, L. J. de Jongh and M. Affronte, *J. Mater. Chem.*, 2006, **16**, 2534–2549.
31. O. Kahn, *Molecular Magnetism,* VCH Publishers, New York (1993).
32. G. Lorusso, V. Corradini, A. Candini, A. Ghirri, R. Biagi, U. del Pennino, S. Carretta, E. Garlatti, P. Santini, G. Amoretti, G. Timco, R. G. Pritchard, R. E. P. Winpenny, and M. Affronte, *Phys. Rev. B*, 2010 , **82**, 144420.
33. S. Carretta, J. van Slageren, T. Guidi, E. Liviotti, C. Mondelli, D. Rovai, A. Cornia, A. L. Dearden, F. Carsughi, M. Affronte, C. D. Frost, R. E. P. Winpenny, D. Gatteschi, G. Amoretti, and R. Caciuffo, *Phys. Rev. B*, 2003, **67**, 094405.
34. A. Ghirri, C. Bonizzoni, M. Righi, F. Fedele, G. Timco, R. Winpenny and M. Affronte, *Appl. Magn. Reson.*, DOI:10.1007/s00723-015-0672-5.
35. G. W. Morley, L.-C. Brunel, and J. van Tol, *Rev. Sci. Instrum.*, 2008, **79**, 064703.
36. L. Krause, R. Herbst-Irmer, G. M. Sheldrick, D. Stalke, *J. Appl. Cryst.* 2015, **48**, 3-10; R. H. Blessing, *Acta Crystallogr.* 1995, **A51**, 33-38.
37. G. M. Sheldrick, *Acta Crystallogr.*, 2015, **C71**, 3-8.

Dalton Transactions RSCPublishing

ARTICLE

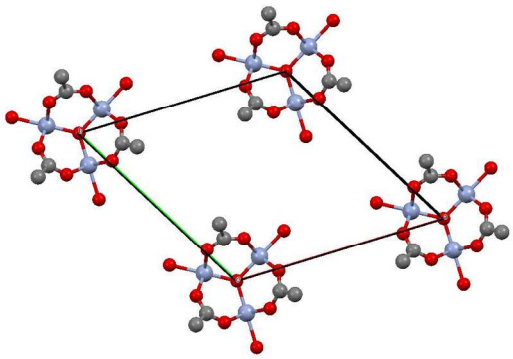

Fig. 1. Crystallographic structure of the Cr_3 crystal. H atoms, CH_3 groups, solvates and non-coordinated pivalate anions excluded for clarity. Colour scheme: Cr, purple; O, red, C, grey.

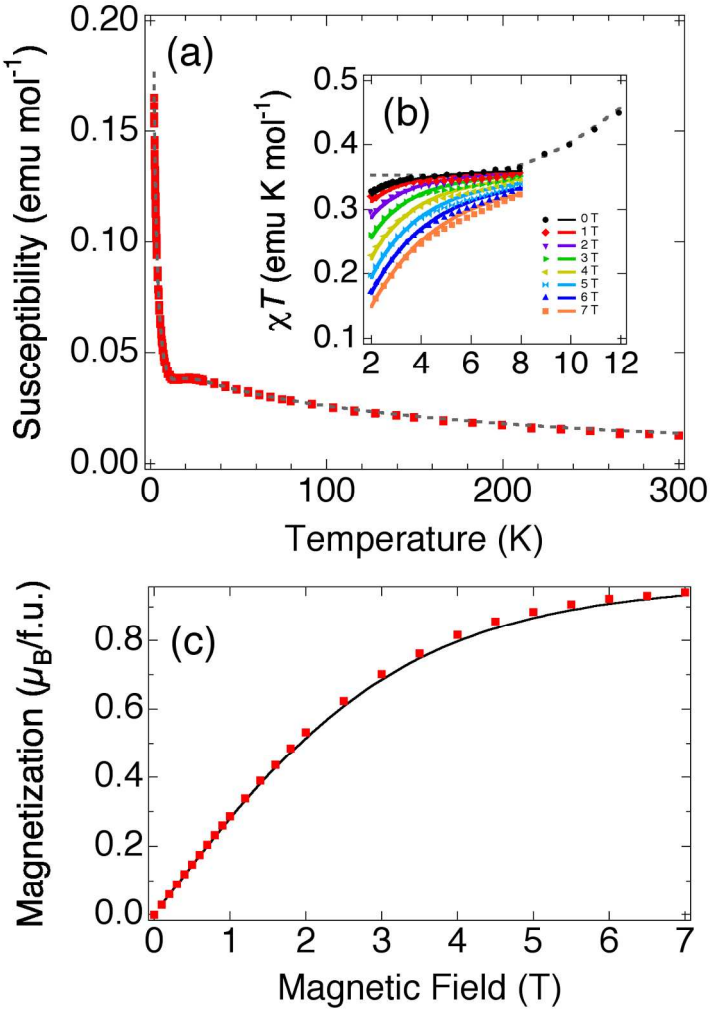

Fig. 2. (a) Susceptibility curve measured on a polycrystalline sample of Cr_3 as a function of the temperature (squares). (b) Magnification of the χT product for $0 \leq B \leq 7$ T. Dashed and solid lines display the calculated curves, respectively with the isotropic and the anisotropic model. (b) Magnetization measured at 2 K (squares) and calculated curve (solid line).

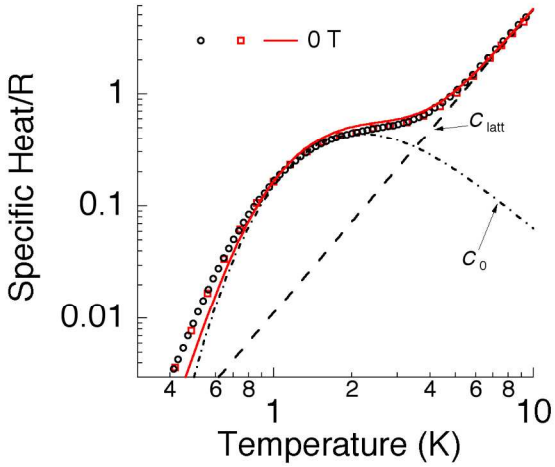

Fig. 3. Zero-field *C*/*R*-vs-*T* curve normalized to the gas constant *R*. Circles and squares show two equivalent sets of data measured with the single crystals oriented along perpendicular directions. The separated contribution of C_{latt} and C_0 are displayed respectively by dashed and dot-dash lines. The solid line represents the curve calculated from Eq. 9.

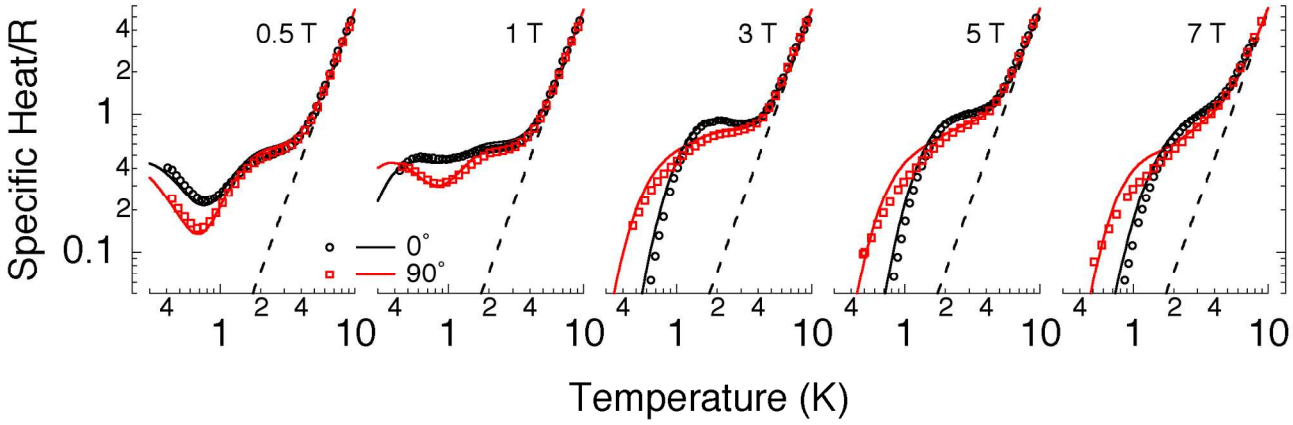

Fig. 4. *C*/*R*-vs-*T* specific heat curves measured at fixed *B*. Black circles and red squares show the experimental data measured respectively for θ=0 and π/2. The dashed line displays the lattice contribution estimated from Eq. 1. Solid lines represent the curves calculated from Eq. 9.

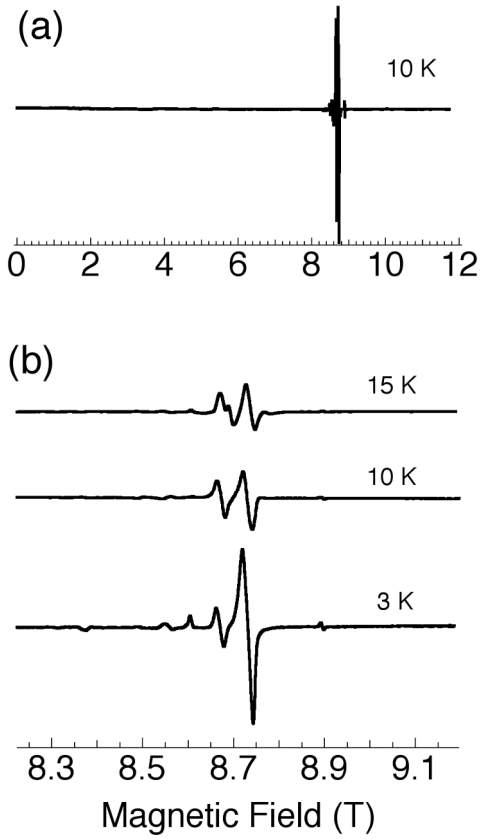

Fig. 5 EPR spectra taken at 240.992 GHz on a single crystal of Cr_3 (θ=0). (a) Field sweep in the range 0-12 T (T=10 K). (b) Temperature dependence of the observed EPR resonances. The saturated signal at 8.60 T corresponds to a $g \simeq g_e$ impurity.

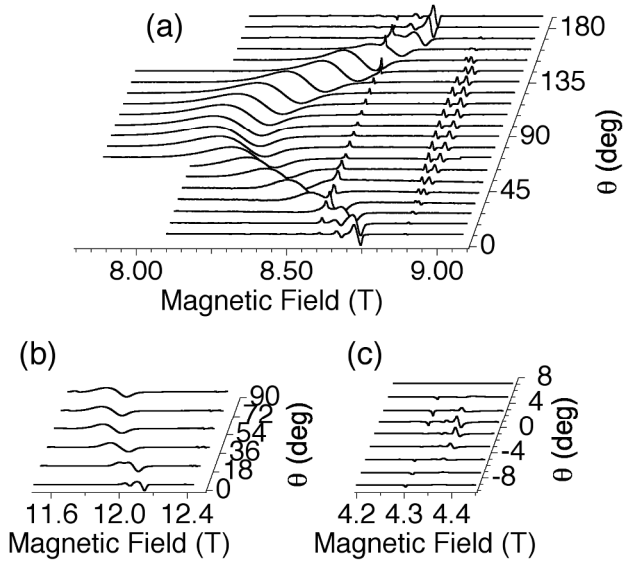

Fig. 6. EPR spectra measured at different θ angles and T=4 K. For each spectrum the intensity is normalized to its maximum value. Microwave frequency: 241 GHz (a); 336 GHz (b); 120 GHz (c).

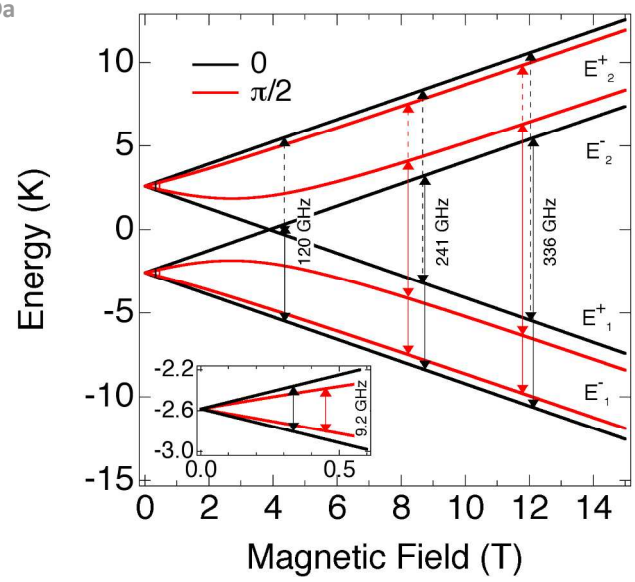

Fig. 7. Energy diagram of the ground state doublets plotted as a function of B for θ=0 and $\pi/2$. Vertical arrows display the position of the observed EPR resonances. Their length corresponds to the energy of the microwave photons $h\upsilon/k_B$, with υ = 9.215, 120.496, 240.992 and 336.000 GHz. Solid and dashed lines respectively show the transitions within lower and higher lying doublets.